Journal of Renewable Energy and Environment

Research Article

Journal Homepage: www.jree.ir

Solar Heat Utilization in Separation Column Reboilers Case Study: Amine Regenerator in South Pars Gas Complex, Assalouyeh

Morteza Keshavarz, Behnam Mostajeran Goortani*

Department of Renewable Energy Engineering, University of Isfahan, Isfahan, Iran.

PAPER INFO

Paper history:
Received 15 Jun 2018
Accepted in revised form 9 September 2018

Keywords:
Non-equilibrium Model
Amine Regenerator
Concentrated Solar heat
Heat Storage
Angstrom Model

ABSTRACT

The amine regenerator of acid removal unit in South Pars Gas Complex, Assalouyeh, Iran was modeled. This model was fitted to assess the large scale columns and allow application of solar thermal energy for production of low pressure steam. Heat transfer fluids including Therminol oil, sulfur, or salt melt could be applied to yield thermal energy from a solar collector and to store and transfer it to the reboiler of columns. The Angstrom model was adopted here to simulate solar irradiance. Solar irradiance data for the city of Assalouyeh, during the years of 2009-2014, were collected and applied. The results indicated that based on a reboiler duty of around 21.8 MW, a solar collector area of 148,000 m^2 was required with a mass of heat transfer and storage medium of 1247255 kg oil, 1787732 kg salt melt and 3803686 kg sulfur, respectively. This model was applied as an analytical tool to explore and describe the following two problems encountered during real plant operation: fouling in the amine heat exchangers and increasing regenerator pressure.

1. INTRODUCTION

Although high volume of solar thermal energy is available in the most parts of the earth, fossil fuels are still the major energy for providing the requirements of different industries. A possible explanation of this drawback is that most industries were born with burning fossil fuels. The increasing in knowledge of researchers in this field regarding renewable sources of heat such as solar may be a solution towards resolution of this drawback. Meanwhile, distillation and regeneration columns consume about 40% of the total energy of these industries [1].

It is necessary to develop methods for energy reduction and move towards sustainable processes. Solar thermal energy is harvested and concentrated through collectors to produce hot water or low pressure steam, the major type of heating source consumed by aforementioned separation processes. Tora et al. studied the integration of solar heat into industrial processes where, hot water tanks are applied to handle the dynamic nature of solar heat and determine the optimal mix of energy types (solar versus fossil) [2]. Integration of parabolic trough solar collectors for production of low pressure steam applied in different industries had been assessed in [3].

*Corresponding Author's Email: b.mostajeran@ast.ui.ac.ir (B. Mostajeran)

Pendaya presented a non-equilibrium model for absorption columns by assuming ideal liquid and vapor phases [4]. Pacheco and Rochell) considered a variable with temperature kinetics for CO_2 absorption inside packed columns [5]. Bolhar et al. assumed two film resistances in the absorption columns [6]. Gabrielsen et al. presented a non-equilibrium model for packed-bed absorption columns assuming equilibrium reactions [7]. Godini and Mowla combined experimental and theoretical studies for examining the absorption of H_2S and CO_2 gasses. They found that although CO_2 is a weak competitor against H_2S, liquid-vapor flow rate ratios are involved in absorption selectivity [8].

Mostajeran et al. presented a flexible three-phase non-equilibrium model for energy efficient reactive distillation columns applied in oil and gas industry [9]. Khan et al. experimentally studied four aqueous amine solvents including MEA, AMP, MDEA, and PZ, as an absorbent for post-combustion CO_2 capture through chemical absorption processes, in a packed column [10]. Yu et al. studied CO_2 absorption process by consuming NH_3/PZ blended solutions in a packed column, and developed and validated a rate-based model for NH_3–PZ–CO_2–H_2O system [11]. Spek et al. developed a model in Procedé Process Software (PPS) environment to study CO_2 capture with a blend of AMP and PZ. This model was a rigorous process simulation model, where the gamma-phi approach was applied to describe vapor-liquid equilibrium (VLE), and the two-film model to

describe reaction kinetics and the diffusion limitations in columns [12].

Several equilibrium and non-equilibrium models have been and are being developed in this field; however, none of the models have been adopted in large scale columns to study the real industrial column and determine the possibility of application of solar thermal energy.

This newly proposed model consists of a six-component non-equilibrium two-phase model with reaction kinetics. Thermodynamic and physical properties of pure component and mixtures in the liquid and vapor phases both as the functions of pressure, temperature, and mole fractions are of concern here. In this study, the variable feature of solar energy that varies in time is considered for this application for the first time. To the knowledge of the authors, the model presents a comprehensive view on solar regeneration columns validated through industrial data.

2. PROCESS DESCRIPTION and UTILIZATION of CONCENTRATED SOLAR HEAT

2.1. Description of the amine absorption process

Amine absorption process removes acidic gases from natural gas, Fig. 1. In this process, natural gas flows into the absorption column, firstly. The absorber feed, a 45% solution of methyl diethanol amine (MDEA), enters the column from the top (s.1) and the sour gas at 25 ^{o}C with 66 bar pressure enters from the bottom (s.2). Amine enters on tray 11 at 40 ^{o}C and exits from tray 34 as a rich amine at the bottom (s.3). H_2S and CO_2 gases are absorbed and the sweet gas exits from the top (s.4).

Some hydrocarbon gases are dissolved in the amine solution because of the high pressure in the column. To regenerate solvent and re-direct the gas flow to the separation process, the above rich amine solution goes through a pressure reduction valve (PRV) with a 58 bar differential pressure. The outlet two-phase stream (s.5) from the valve enters a flash drum where two liquid and gas streams, s6 and s.7, are separated. The liquid stream is heated up to 97 ^{o}C in amine exchanger and enters the regenerator tower (s.8). The regenerator column pressure is 2.2 bar at the top and 2.6 bar at the bottom. At this column temperature and pressure, the dissolved acidic gas is stripped and separated from the column at the top (s.9). The bottom product of amine regenerator (s.14) is directed into the reboiler where it is heated and the water fraction is changed into the vapor. The vapor stream (s.15) is re-routed to the amine regenerator column where it is stripped and the acidic gas is separated from the amine. The outlet liquid from the reboiler (s.16) returns to the column. The regenerated amine solvent exits from the bottom of column at 132 ^{o}C (s.10) and then it is directed to the amine heat exchanger and heats the water liquid stream flash drum outlet (s.7). The lean amine is cooled to 40 ^{o}C after passing through amine cooler and exchanging heat with sea water (s.17). This solvent is stored in amine tank and the cycle is repeated. The acidic gases leave the column at 105 ^{o}C from the top (s.9). To separate water from amine, this stream first enters air coolers and exits as vapor-liquid at 65 ^{o}C towards the reflux drum (s.11). The acidic gases from the top (s.12) enter the sulfur recovery unit 108 and the liquid is pumped to the amine regenerator as reflux (s.13).

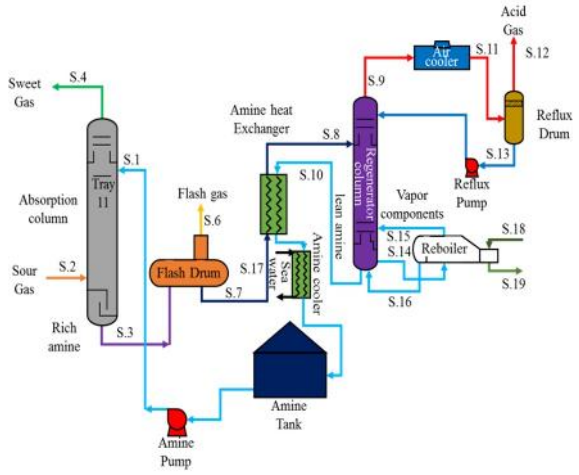

Figure 1. The scheme of acidic gases removal from natural gas, the amine absorption process

The amine regenerator column is composed of 25 valve trays. The regenerator feed enters tray five. The average feed composition, temperature, and pressure, are tabulated in Table 1. About 85% of the feed is water, mainly to facilitate heat transfer in the column.

TABLE 1. Specifications of the feed inlet to the regenerator column

Parameter	Value
Flow rate (kmol/s) - CO_2 - H_2S - H_2O - MDEA	 0.073 0.053 2.69 0.33
Pressure (bar) Temperature (^{o}C)	2.4 103

2.2. Utilizing stored solar thermal energy in the regenerator column

The process of applying solar thermal energy in the amine regenerator and replacing the existing fossil fuel process is illustrated in Fig. 2. In this figure, the condensate from the reboiler (s.19) enters the heat exchanger of the solar thermal heat storage system. The heat transfer fluid provides heat to its condensate to be converted into vapor as low pressure (LP) steam (s.18) and to be directed back to the reboiler. The heat transfer

fluid is sent to a cold tank (s.20), and then to the receiver of the solar collectors (s.21), where it receives thermal energy. Finally, it is sent to the hot tank (s.22).

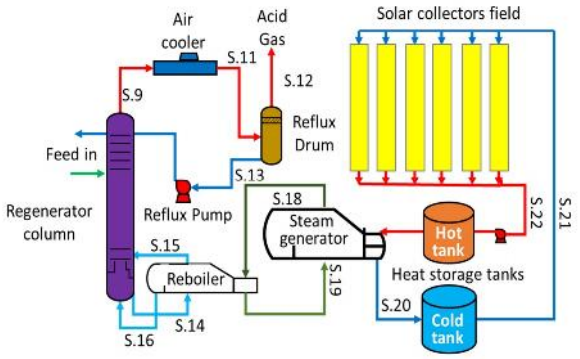

Figure 2. The scheme of utilizing solar thermal energy in amine regenerator reboiler

To design solar amine regenerator, first a non-equilibrium model is developed in gPROMS environment. The two-phase, multi-component mass and energy balances are developed for the reboiler,trays, and air cooler. This model is validated through the operational data of the industrial column. It is necessary to have a reliable model for describing the solar irradiance; therefore, the data are applied received from a weather station in the city of Assalouyeh from 2009 to 2014. To utilize solar energy during night or cloudy days, appropriate storage tanks are designed based on 12 working hours of storage.

3. MODEL DEVELOPMENT

Three models are developed at the initial phase: for calculating the multi-component mass and energy transfer coefficients, for energy and mass balance equations over air cooler, trays, and reboiler, and calculating solar irradiance, collector area, and process parameters of the heat storage system.

TABLE 2. Multicomponent mass and heat transfer coefficients applied in this model

Coefficient	Correlation
Liquid phase mass transfer coefficient	$k_{i,j}^{L} = 125(Re^{V})^{0.684}(Re^{L})^{0.087}h_{w}'^{0.051}(Sc^{L})^{0.5}D_{i,j}^{L}A_b/a_t$ [15]
Vapor phase mass transfer coefficient	$k_{i,j}^{V} = 9.93(Re^{V})^{0.865}(Re^{L})^{0.130}h_{w}'^{0.389}(Sc^{V})^{0.5}D_{i,j}^{V}A_b/a_t$ [15] $a_t = 0.27A_b(Re^{V})^{0.375}(Re^{L})^{0.247}h_{w}^{0.515}$ $h_w' = h_w/d$
Liquid phase heat transfer coefficient	$h_i^L = k_i^L \rho_i^L cp_i^L \left(\frac{\lambda_i^L}{\rho_i^L c_i^L D_{ave}^L}\right)^{2/3}$ [30]
Vapor phase heat transfer coefficient	$h_i^V = k_i^V \rho_i^V cp_i^V \left(\frac{\lambda_i^V}{\rho_i^V c_i^V D_{ave}^V}\right)^{2/3}$ [30]
Average liquid phase mass transfer coefficient	$k_{ave}^{L} = \left(\sum_{i=1}^{NC} k_{i,j}^{L}\right)/NC$
Average vapor phase mass transfer coefficient	$k_{ave}^{V} = \left(\sum_{i=1}^{NC} k_{i,j}^{V}\right)/NC$
Average diffusion for liquid phase	$D_{ave}^{L} = \left(\sum_{i=1}^{NC} D_{i,j}^{L}\right)/NC * NC$
Average diffusion for vapor phase	$D_{ave}^{V} = \left(\sum_{i=1}^{NC} D_{i,j}^{V}\right)/NC * NC$

3.1. Multi-component mass and energy transfer coefficients

There exist many experimental and theoretical correlations in predicting mass and heat transfer coefficients in liquid and vapor phases. According to Sherwood and Holloway correlation, the the major resistance is in the liquid phase [13]. Onda et al. assumed a resistance for the gas phase as well [14]. They illustrated that at their best their correlations describe the experimental data. Kim and Deshusses modified Onda correlations by adding power of i to Reynolds number, and replaced the numerical constant with variable c [15]. Scheffe and Weiland assumed the coefficients tabulated in their study for the mass transfer

correlations applied in this study as tabulated in formulations in Table 2 [16]. The symbols applied in all equations are defined in the nomenclature at the end of this manuscript. For calculating the heat transfer coefficient in liquid h_i^L and in vapor h_i^V phases, the Cluboron-Chilton analogy is applied.

3.2. Energy and mass balance equations of condenser, trays, and reboiler models

3.2.1. Air cooler model

The inlet and outlet stream flows to the air cooler as shown in Figs. 2 and 3, where the vapor stream from tray 2 (s.9) enters the air cooler, loses its thermal energy, Q_c, and leaves the air cooler as vapor, V_1. The liquid stream returns completely to tray 2 as reflux. In the energy equation of the air cooler, the heat loss is assumed to be 10% of the total air cooler duty, Q_c. It is assumed that the outlet streams from air cooler are in thermodynamic equilibrium.

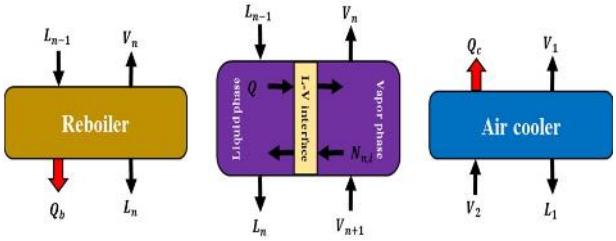

Figure 3. Schematic illustration of the mass and energy inputs and outputs for air cooler, trays, and reboiler

3.2.2. Trays Model

Energy and mass balances in the liquid and vapor phases over tray *n* are reported in Table 3. All physical and thermodynamic properties of pure components and mixtures in vapor and liquid phases are calculated in this model which is assumed to be a function of temperature, pressure, and composition.

TABLE 3. Multicomponent two-phase mass and energy balances applied in the model

Condenser (n=1)	Mass balance	$y_{2,i} * V_2 - y_{1,i} * V_1 - x_{1,i} * L_1 = 0$ i=A, B,…, NC $x_{1,i} = \alpha_{1,i} * y_{1,i}$
	Energy Balance	$\sum_{i=A}^{NC} V_2 * \text{Vapour enthalpy}(T_2, P_2, y_{2,i}) - Q_c - \sum_{i=A}^{NC} V_1 * \text{Vapour enthalpy}(T_1, P_1, y_{1,i}) - \sum_{i=A}^{NC} L_1 * \text{Liquid enthalpy}(T_1, P_1, x_{1,i}) - Q_{loss} = 0$
Trays (n = 2….24)	Mass balance	$Vapor\ phase:\ y_{n+1,i} * V_{n+1} + N_{n,i} - y_{n,i} * V_n = 0$ $Liquidphase:\ x_{n,i} * L_n - N_{n,i} - x_{n+1,i} * L_{n+1} - R_{n,i} = 0$ $x_{n,i} = \alpha_{n,i} * y_{n,i}$
	Energy Balance	$Vapor\ phase:\ \sum_{i=A}^{NC} V_{n+1} * Vapour enthal\ py(T_{V_{n+1}}, P_{V_{n+1}}, y_{n+1,i}) + h^V * (T_{V_n} - T_{l_n}) - \sum_{i=A}^{NC} V_n * Vapour enthal\ py(T_{V_n}, P_{V_n}, y_{n,i}) - \sum_{i=A}^{NC} N_{n,i} * Vapour enthal\ py(T_{V_n}, P_{V_n}, y_{n,i}) = 0$ $Liquidphase:\ \sum_{i=A}^{NC} L_{n-1} * Liquidenthal\ py(T_{L_{n-1}}, P_{L_{n-1}}, x_{n-1,i}) - h^L * (T_{L_n} - T_{l_n}) + Reaction\ heat - \sum_{i=A}^{NC} L_n * Liquidenthal\ py(T_{L_n}, P_{L_n}, x_{n,i}) + \sum_{i=A}^{NC} N_{n,i} * Liquidenthal\ py(T_{L_n}, P_{L_n}, x_{n,i}) = 0$
Reboiler (n=25)	Mass balance	$L_{n-1} - L_n - V_n = 0$ $x_{25,i} = \alpha_{25,i} * y_{25,i}$
	Energy Balance	$\sum_{i=A}^{NC} L_{n-1} * Liquidenthal\ py(T_{n-1}, P_{n-1}, x_{n-1,i}) - \sum_{i=A}^{NC} L_n * Liquidenthal\ py(T_n, P_n, x_{n,i}) + Q_{reb} - Q_{loss} - \sum_{i=A}^{NC} V_n * Vapour enthal\ py(T_n, P_n, y_{n,i}) = 0$

The variable $\alpha_{n,i}$ the distribution coefficient at the vapor-liquid interface in tray *n*, is calculated through Eq. (1):

$$\alpha_{n,i} = \varphi^V / \varphi^L \quad (1)$$

Where, φ^V and φ^L are the vapor fugacity coefficient and liquid fugacity coefficient, respectively.

CO_2 absorption, in the first and second types of amines, occurs quickly and reaches equilibrium, while absorption in the third amine, methyl diethanol amine,

occurs slowly. The reason is that first CO_2 is dissolved in water to produce bicarbonate. Also, the bicarbonate reacts with water. Pacheco and Rochelle applied the following reaction rates [5]:

$$R_{MDEA} = k_{2t}[CO_2][MDEA] - \left(k_{2t}/K_{2t}\right)[MDEA^+][HCO_3^-] \quad (2)$$

$$k_{2t} = 2.576 \times 10^9 exp\{-6024/T\} \quad (3)$$

Where,parameters $[CO_2]$, $[MDEA]$, $[MDEA^+]$, and $[HCO_3^-]$ are the concentrations of the components and T is the temperature. For the molar fluxes of liquid and gas phases, $N_{n,ji}$ is expressed as:

$$N_{n,i} = k_{ave}^L\left(x_{n,i}^I - x_{n,i}^L\right) = k_{ave}^V\left(y_{n,i}^V - y_{n,i}^I\right) \quad i,j = A,B,\dots,NC \quad (4)$$

Where, parameters k_{ave}^L and k_{ave}^V are the multicomponent mass transfer coefficients in liquid and vapor phases, respectively. Variables $x_{n,i}^I$, $x_{n,i}^L$ $y_{n,i}^V$, and $y_{n,i}^I$ represent the composition of component i in liquid interface, bulk liquid, bulk vapor, and vapor interface, respectively.

The diagrams in [5] are applied here in determining the reaction heat between acidic gases and amine solution.

The overall energy balance, between liquid and vapor phases, is expressed as:

$$h^V * (T_V - T_I) = h^l * (T_I - T_L) \quad (5)$$

Where, h^V and h^l are the vapor and liquid heat transfer coefficients obtained from Cluboron-Chilton analogy, respectively (Table 2).

3.2.3. Reboiler model

As observed in Figs. 2 and 3, the liquid stream outlet from the last tray (s.14) L_{n-1} enters reboiler (n), where it receives Q_b and is changed into vapor stream (s.15) V_n and liquid, lean amine. Mass and energy balance are tabulated in Table 3. It is assumed that heat losses in the reboiler are 10% of the reboiler duty and the outlet streams from the boiler are in thermodynamic equilibrium.

3.3. Solar model

3.3.1. Solar irradiance model

Solar irradiance is a variable with time parameter, depending on geographical location, date, time of the day, and weather conditions. Correlations describing this parameter are complex, and thus only a number of solar parameters such as the number of sunny hours, relative humidity (RH), latitude, and temperature are applied in the correlations [17, 18]. The number of sunny hours is applied by many researchers in the experimental correlations [19]. Lashkar Ara et al. estimated the monthly average of daily global solar irradiance on a horizontal surface in different regions of Iran by a new method based on empirical equations and ant colony optimization algorithm [20]. Also, Yaghoubi applied the number of sunny hours to obtain transmission coefficient for the city of Shiraz [21].

In one of the recent studies, the effect of cloud properties has been assessed on solar irradiance through satellite observations [22]. Stefu et al. modified the Angestrom equation based on the effect of shadow by applying long term records of global solar irradiation registered in 13 stations in EU [23].

Vakili et al. assessed the effect of particulate matter pollution on estimation of daily global solar radiation by applying ANN modeling based on meteorological data [24]. The solar irradiance model applied in this study is of the third order Angstrom model defined by:

$$\frac{H}{H_0} = a + b\left(\frac{S}{S_0}\right) + c\left(\frac{S}{S_0}\right)^2 + d\left(\frac{S}{S_0}\right)^3 \quad (6)$$

The parameter H_0 is the solar irradiance outside atmosphere calculated in accordance with Table 4. Here, parameters δ and φ represent the latitude and sun declination angle, respectively. Applying the solar irradiance data provided from Assalouyeh weather station for the years of 2009-2014 by linear regression method and the constants of the equation are calculated and the results are tabulated in Table 5.

TABLE 4. Equations used in this model for estimation of solar irradiance

Variable	Equation
Declination angle (δ)	$\delta = 23.45\sin(360(N+284)/365)$
Sunset angle ($\omega_{su\ nset}$)	$\omega_{su\ nset} = \cos^{-1}(-\tan\delta\tan\varphi)$
Day length (h)	Day length $= 2\omega_{su\ nset}/15$
Solar irradiance outside atmosphere (H_0)	$H_o = H_{sc}\left(1 + 0.034\cos\left(\frac{360N}{365.25}\right)\right) \times \left(\cos\varphi\cos\delta\sin\omega_{su\ nset} + \frac{\pi \times \omega_{su\ nset}}{180}\sin\varphi\sin\delta\right)$

TABLE 5. Constants of the third-order Angstrom model obtained for Assalouyeh

Constant	R^2	d	c	b	a
Value	0.9716	661.58	2443.7	3001.2	0.1225

3.3.2. Solar heat storage model

To utilize thermal solar energy during night and cloudy hours, application of heat storage tanks is a must. Differential equations are applied in calculating storage tanks parameters (Table 6). Parameters of M_{hot}, T_{hot}, M_{cold}, and T_{cold} represent the mass and temperature of both hot and cold tanks, respectively. Parameters $\dot{m}_{col}$ and $\dot{m}_{reb}$ are the mass flow rates of the heat transfer medium in the collector and low pressure (LP) steam generator, respectively. In Table 6, w_{sunset} is the sunset hour angle in degrees and t_{sunset} and $t_{sunrise}$ denote the sunset and sunrise times, respectively.

TABLE 6. Transient mass and energy balances applied in solar heat collection and storage model

$\dot{m}_{reb} - \dot{m}_{col} = (dm_{cold})/dt$
$\dot{m}_{col} - \dot{m}_{reb} = dm_{hot}/dt$ $d(m_{hot} * T_{hot})/dt = \dot{m}_{col} * T_{col} - \dot{m}_{reb} * T_{hot}$
$d(m_{cold} * T_{cold})/dt = \dot{m}_{reb} * T_{reb} - \dot{m}_{col} * T_{cold}$
$\int_{t_{sunrise}+1}^{t_{sunset}-1} H * \eta * \text{Area} * Q_{reb} dt = 24 * 3600 * Q_{reb}$ $\dot{m}_{col} * cp * (T_{col} - T_{cold}) = H * \eta * \text{Area}$ $w_{su\ nset} = Acos(-tan(r * \delta) * tan(r * \varphi))/r$ $t_{su\ nset} = 12 + w_{su\ nset}/15$ $t_{su\ nrise} = 12 - w_{su\ nset}/15$ $m_{cold} + m_{hot} = \dot{m}_{reb} * (t_{su\ nrise} - t_{su\ nset} - 2) * 3600$ $m_{cold} + m_{hot} = \dot{m}_{reb} * (t_{su\ nrise} - t_{su\ nset} - 2) * 3600$

Where, parameters δ and φ show latitude and sun declination angle, respectively.

The heat intake capacity of these storages depends on the time required for the operation of the reboiler without sun. This duration is very important as it affects the cost analysis results. The number of sunny hours of a day changes during the year. Consequently, to determine this capacity, the design should be based on the shortest sunny day of the year. During cloudy hours, the system should switch to fossil fuel consumption. For the city of Assalouyeh, according to Fig. 11, the shortest sunny day is 10 hours and 17 minutes for Assalouyeh on December 20. However, due to the financial restrictions regarding large storage capacities, the design calculations of this study are based on 12 hours storage.

The reboiler duty, Q_{reb}, is 21.8 MW and the storage system should provide this thermal load during 12 hours:

$$Q_{reb} * 12 * 3600 = \int_{t_{sunrise+1}}^{t_{sunset-1}} area * \eta * H * dt \quad (7)$$

Where, the area is the collector area, η represents the solar collector overall efficiency (assumed to be 70%), and H denotes the solar energy intensity. According to this equation, the required collector area is 148000 m^2.

3.4. Development of the model equations in gPROMS environment

The gPROMS software is an advanced modeling tool applied in modeling mass and energy balances of the equipment and processes subject to transient or steady state conditions. This software is mainly applied in oil and gas research [9]. Together with Multiflash and the data banks of material properties, this software is equation-oriented and allows user to write appropriate equations and solve them simultaneously by assuming the variable physical and thermodynamic properties of the materials. These equations are applied in calculating the properties for pure components and mixtures, in vapor and liquid phases, where are all presented as functions of pressure, temperature, and components fractions.

Mass and energy balances are presented and solved in gPROMS simultaneously. The physical and thermodynamic properties of liquid and vapor phases are calculated through Multiflash, software for calculating of physical and thermodynamic properties. Different thermodynamic and physical property models are applied in this model in the vapor and liquid phases, Table 7 [25, 26, 27].

TABLE 7. Applied correlations to calculate thermodynamic and physical properties of pure components

Parameter	Equation
Equation of state	$P = \frac{NRT}{V-b} + \frac{a}{V^2 + 2bV - b^2}$
Binary diffusion coefficient	$D_{ij} = \frac{1.0112 \times 10^{-22} T^{1.75} K_{ij}}{P\left(\left(\sum_i^{1/3} + \sum_j^{1/3}\right)\right)^2}\left(\frac{1}{M_i} + \frac{1}{M_j}\right)^{1/2}$
Specific heat	$\frac{c_P}{R} = a_1 + (b_1 - a_1)y^2(1 + (y-1)F(y))$
Density	$\rho = \frac{1}{V_c} + a_2 T^{1/3} + b_2 T^{2/3} + c_2 T + d_2 T^{4/3}$
Thermal conductivity	$\lambda = a_3(1 + b_3 T^{1/3} + c_3 T^{2/3} + d_3 T)$

To calculate the different physical and thermodynamic properties for mixtures and pure components (e.g. enthalpy, entropy, fugacity, fugacity coefficient, density and …), temperature, pressure, and composition should be specified. For example to calculate the vapor mixture fugacity coefficient, φ^v, the following equation is written in gPROMS program:

$$\varphi^v = \text{vapor fugacity coeficient}\left(T_{V_n}, P_n, y_{n,i}\right) \quad (8)$$

Where, $T_{V_n}, P_n, \text{and } y_{n,i}$ are the vapor temperature, pressure, and composition, respectively, at stage n.

3.5. Model validation

To validate the results of this model mass balance, the industrial mass balance data for the top (air cooler) and the bottom (reboiler) of the amine regenerator column are applied. The components H_2S, CO_2, and H_2O exit from the top, while amine and water solution exit from the bottom of the column. The simulation results are compared with the data presented in Table 8.

TABLE 8. Stream compositions at the top and bottom of amine regenerato

Error (%)	Model results	industrial data	Parameter
Top			
CO_2	0.925	0.5417	0.54
H_2S	1.38	0.3625	0.36
H_2O	4.2	0.958	0.10
MDEA	0	0.0	0.0
Bottom			
CO_2	6.6	0.0224	0.021
H_2S	5.7	0.0222	0.021
H_2O	0.4	0.8466	0.85
MDEA	0.9	0.109	0.11

To calculate the error, Eq. (9) is applied:

$$e_{relative} = \frac{\text{calculated model results} - \text{industrial data}}{\text{industrial data}} * 100 \quad (9)$$

The industrial data applied here consist of available plant manuals and data sheets.According to Table 8, the determined error is less than 6% in prediction of composition from the top and bottom of the column. The vapor phase compositions of CO_2, H_2S, and H_2O along the column are shown in Fig. 4. According to this figure, the composition of water vapor is 73% at the top, which is condensed and returned to the column as reflux.

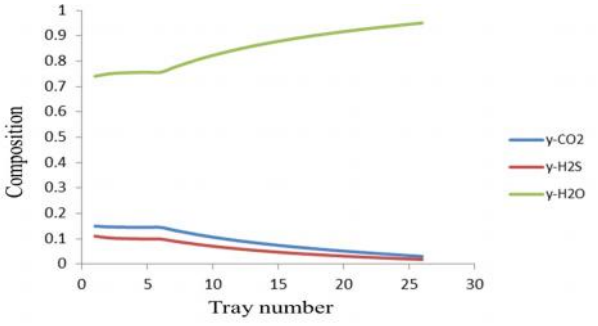

Figure 4. Vapor phase compositions of CO_2, H_2S, and H_2O through the column

The feed enters the column at 103 °C, at top temperature of 112°C and bottom temperature of 132°C. The comparisons of temperature at the top and bottom in this model with those of the experimental data are expressed in Table 9.

TABLE 9. Comparison of temperature at the top and bottom of the column

Location	Industrial data	Model	Error (%)
Feed	103	103	-
Column top	112	111.8	0.178
Column bottom	128	128.5	0.39
Reboiler	132	132.5	0.384

The temperature of the liquid-vapor interface along the column is shown in Fig. 5, where there is a change in the slope at tray 5 because of feed injection. In the last tray, the interface temperature is slightly higher than that of bulk liquid due to the entrance of reboiler vapors. Also, the interface temperature at the first tray is slightly lower than that of bulk liquid due to colder liquid entry from the air cooler.

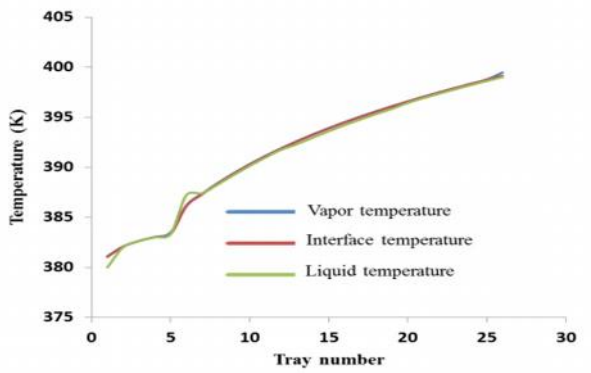

Figure 5. Profiles of temperature along the column in the liquid, vapor, and vapor-liquid interface

The volume of the vaporized liquid depends on boil up ratio, assumed to be 0.2. The volume of reflux depends on air cooler duty. Reflux ratio is assumed to be 0 (Table 10).

TABLE 10. Comparison of the model results with experimental data: condenser and reboiler duties

Parameter	Industrial data	Model results	Error (%)
Reboiler duty (MW)	21.774	21.3561	0.74
Air cooler duty (MW)	14.30	14.7024	2.8

4. PARAMETRIC ANALYSIS OF THE REGENERATOR WITH SOLAR REBOILER

Based on the observations made on experiences under real operation of the column, the following two parametric analyses are presented: the effect of an increase in air cooler and reflux drum pressure on the

mass and the energy balance, and the effect of feed temperature.

4.1. Increasing air cooler and reflux drum pressure

In this analysis, air cooler and reflux drum pressure grows from 1.8 bar to 2.2 bar. During the real operation of the plant, this occurs when there is a problem in transfer, where CO_2 and H_2S gases enter unit 108, i.e. the reception unit of sour gases. Vapor boil up ratio is not changed in the first part of this analysis. Because of an increase in the reflux drum pressure, the column and reboiler pressures rise; consequently, water vapors decrease at the top of the column (Fig. 6).

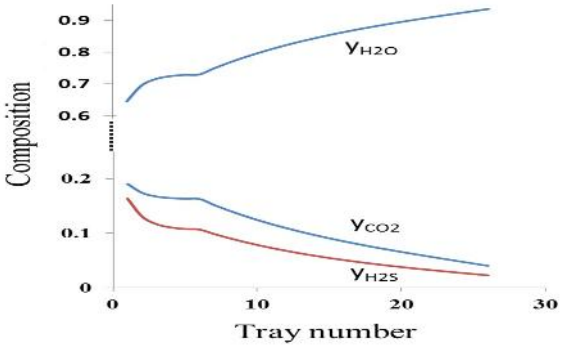

Figure 6. Mole fraction profiles along the column at p = 2.2 bar

Elevation of the column pressure increases the reboiler pressure whereby temperature rises. As observed in Fig. 7, the reboiler temperature increases from 399 K to 404 K, while the amount of water vapor at top of the column is not sufficient. The boil-up ratio (BR) in the reboiler should be enhanced in order to have sufficient reflux and appropriate water volume at the top.

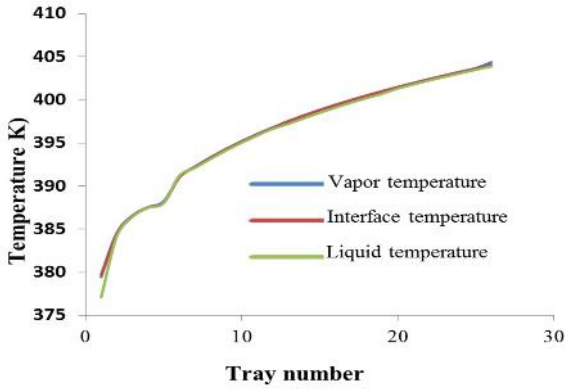

Figure 7. Temperature profile along the column at 2.2 bar condenser pressure

It is observed that an increase in reflux drum pressure and a constant BR reduce the water volume and reflux at the top. To increase this reflux, the BR should be augmented from 0.21 to 0.235, consequently, the reboiler duty should be raised from 21.41 MW to 23.237 MW (i.e. there is 1827 kW increase in the reboiler duty). Compositions of H_2S and CO_2 decrease because of an increase in water composition at the top. This leads to addition of water in the amine storage tank in order to keep the amount of amine constant during recirculation. By increasing the pressure and column BR, the temperature grows. In comparison to the standard conditions, temperature rises by about 6 ^oC. In comparison to the pressurized conditions, temperature grows by about 1.5 ^oC.

4.2. Decreasing feed temperature

Here the temperature of the feed diminishes from 373 K to 363 K. This reduction occurs when there is fouling in the amine heat exchangers. The mole fractions along the column are shown in Fig. 8.

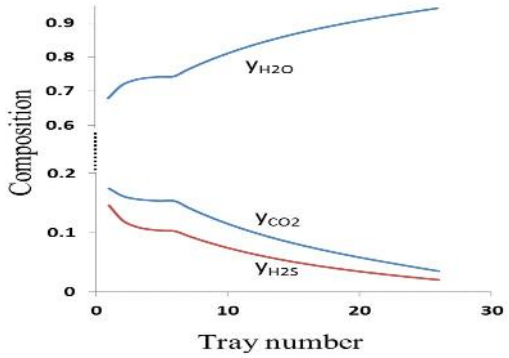

Figure 8. Column composition profile at 10 ^oC reduction in the feed temperature

When BR is constant and feed temperature is low, the water composition at the top of the column decreases with a drop in reflux volume. To enhance the reflux to its standard conditions (0.37 kmol/s), BR should be raised from 0.21 to 0.24; consequently, the reboiler duty increases from 21.41 MW to 24.143 MW. This is a significant growth in reboiler duty. By increasing BR to 0.24, 4 ^oC increase is observed at the column bottom.

4.3. Mass flow rate in the solar collector receiver

The total heat losses are assumed to be 20%. Based on 100 ^oC temperature increase in solar collectors (from 180 ^oC to 280 ^oC), the mass flow rate of heat transfer medium in the collector $\dot{m}_{col}$ is obtained through Eq. (10):

$$\dot{m}_{col} = \frac{H \times 148000 \times 0.7 - 26.1288}{c_p \times 100} \quad (10)$$

Where, H is the instantaneous solar irradiance for the shortest day of the year, calculated according to Fig. 9. The calculations are performed for three types of storage medium: heat transfer oil, sulfur, and salt melt. The mass flow rate of the medium with respect to time is diagrammed in Fig. 10.

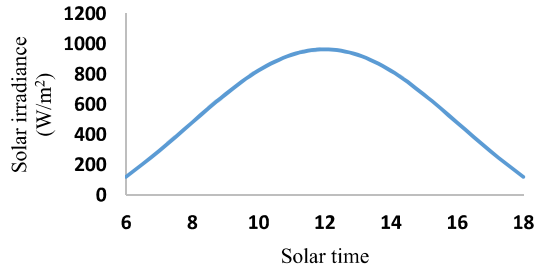

Figure 9. Solar irradiance changes during the shortest day of the year in Assalouyeh

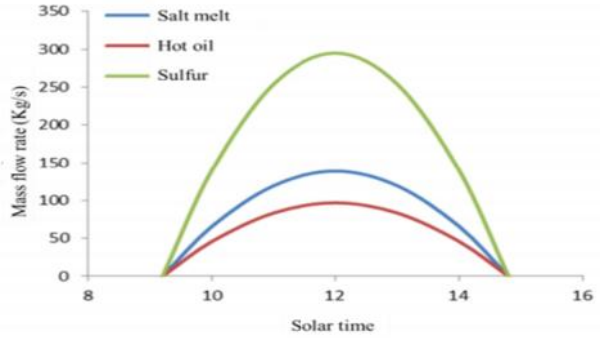

Figure 10. Mass flow rate in the receiver of solar collector for sulfur, hot oil, and salt melt

A heat storage system should be applied in storing solar thermal energy during 12 hours of a day. The storage capacity depends on the number of sunny hours during a day.

To ensure permanent plant operation during a year, the storage system should be capable of storing solar heat during the shortest day of the year. For the cloudy days, the system should shift to fossil fuel consumption. The difference between sunset -1 and sunrise +1 is the number of sunny hours. The solar hour angle is calculated for sunset, w_{sunset} for all the days of the year. The day length is determined in Fig. 11. For Assalouyeh, December 20 has the minimum length of 10 h and 17 minutes. However, because of large heat capacity requirements, the calculations are made based on 12 h of heat storage.

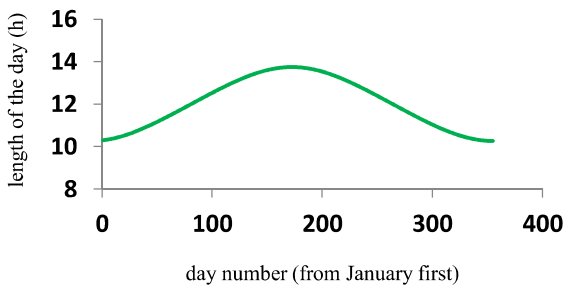

Figure 11. Day length during year

4.4. Solar heat storage tank levels

The reboiler needs 21.8 MW heat and the storage system should provide this heat during the absence of sun. To calculate the mass flow rate in the receiver of the collector, the required variation of solar irradiance during December 20 is applied.

The collector heat is calculated through Eq. (11):

$$Q_{col} = H \times A \times \eta \quad (11)$$

Where, η is the collector's overall efficiency, assumed as 0.70 [28] and A is the required area, calculated as 148,000 m^2. To calculate the necessary heat, Eq. (12) is applied:

$$Q_{col} - Q_{reb} - Q_{loss} = Q_{storage} \quad (12)$$

The outlet temperature from collector and cold tank is assumed as 280 °C and 180 °C, respectively. Accordingly, the mass flow rate to the collector, $\dot{m}_{storage}$, and to the hot tank is obtained through Eq. (13):

$$Q_{storage} = \dot{m}_{storage} \times c_p \times (T_2 - T_1) \quad (13)$$

The area below mass flow rate diagram represents the total mass of the heat storage medium (Fig. 10). This total mass is calculated for the three storage media (Table 11). The variations of hot tank mass for the three fluids in the diagram during the day are presented in Fig. 12, where the accumulation of mass during the day is also expressed.

TABLE 11. Total capacity of tanks for heat storage

Fluid	Total mass (kg)
Hot oil	1247255
Salt melt	1787732
Sulfur	3803686.1

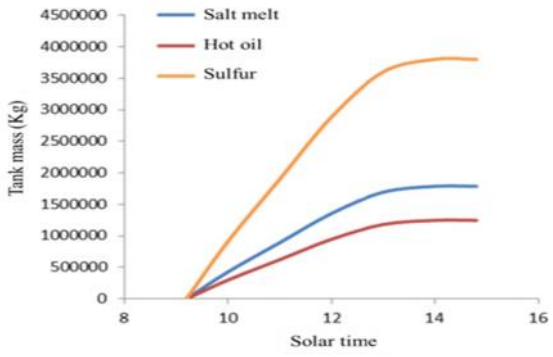

Figure12. Variations of storage tank masses during the day

The result of this analysis is tabulated in Table 12, where the unit and the total costs for the collector, heat

storage system, and natural gas are presented as well. The unit prices of the equipment have been taken from Cocco and Serra [29].

TABLE 12. Cost list for the proposed solar heat collection and storage system

Item	Unit cost	Total cost
Solar collector	177\$/m^2	26.20 M\$
Heat Storage system		
Hot oil	2.7\$/kg	3.368 M\$
Storage tanks	220\$	315340 \$
Piping	33\$/m	4.852 M\$
Heat exchangers	5M\$	5 M\$
Engineering	20% of total cost	2.707
Total		**16.24 M\$**
Natural gas	350\$/1000m^3	4.59 M\$/year

Daily average solar heat consumption is assumed to be 12 h for the calculations of collectors and storage tanks; therefore, the fossil fuel is considered as half in this cost analysis.

The amount of natural gas necessary in the boiler, Q_{NG}, is calculated from boiler capacity, 21.7 MW, and assuming a heating value of 35 MJ/m^3 and an overal efficiency of 0.9:

Q_{NG} = 26.16 MW /2*(3600*24*365)/(35 /0.9 = 13.1*10^6 m^3/year.

No carbon dioxide is released by the solar reboiler, thus, total savings in the carbon taxes, *S,* is:

S= \$0.023/ m^{3}CO$_2$ *13.1 *0.7(kgNG/m^{3}NG)*3 (kgCO$_2$/kgNG)/1.98(kgCO$_2$/m^{3}CO$_2$) = \$0.32M

Simple payback time is defined by the following equation:

$$PBT = I/(R+S) \quad (14)$$

The parameters I, R, and S represent the total investment (M\$), revenue (M\$/year), and savings (M\$/year), respectively. Accordingly, by inserting these parameters in Eq. (14), the following is obtained:

PBT = (26.2+16.24)/(4.59+0.32) = 8.6 years

These calculations indicate that a total investment of 42.44 M\$ is necessary to upgrade the fossil fuel based reboiler of the amine regenerator by replacing it with a solar-based reboiler. This replacement prevents the release of around 27000 tons/year of CO_2 into atmosphere. *PBT* here has been calculated ignoring factors such as carbon taxes/negative environmental impacts of using cheap natural gas. Applying these factors would lead to lower values of *PBT* with the same investment. For example, assuming 25\$ carbon tax per tons of CO_2 release, a *PBT* of 7.6 years is obtained.

6. CONCLUSION

A six-component non-equilibrium two-phase solar model is developed and proposed for the real-scale amine regenerator in South Pars Gas Complex, Assalouyeh, Iran. The thermodynamic and physical properties of pure component and mixtures in the liquid and vapor phases, as the functions of pressure, temperature and mole fractions, are considered in this model. This model is validated through the available industrial data of the column. This model is adopted as a diagnostic tool to explore the two problems encountered during plant operation: fouling in heat exchangers and unexpected entrance of sour gases into the unit. The effects made on column's condenser pressure and feed inlet are in line with these two operational problems. The possibility of utilizing concentrated solar thermal collectors with 12 h of heat storage tanks is discussed here to provide the thermal energy required for the generation of MP steam in the reboiler of the column. The results predict a total collector area of 148,000 m^2. The possibility of applying three heat storage media, the hot oil, salt melt, and sulfur are studied. The masses of heat transfer and storage medium are 1247255 kg of oil, 1787732 kg of salt melt, or 3803686 kg of sulfur, respectively. A total investment of 42.44 M\$ is necessary to upgrade the fossil-fuel-based reboiler of the amine regenerator by replacing the existing system with a solar-based reboiler. This upgrading would prevent the release of around 27000 tons/year of CO_2 into atmosphere. The predicted payback time is 8.6 years.

7. ACKNOWLEDGEMENT

This study is supported R&D department of South Pars Gas Complex (contract no. 306084). The authors acknowledge the contribution of the vice chancellor of research department at University of Isfahan.

NOMENCLATURE:

A_b	Total active bubbling area on the tray (m^2)
ANN	Artificial neural network
a_t	Total interfacial area for mass transfer (m^2)
a_i, b_i, c_i, d_i	Used coefficients for the calculation of physical properties of pure component
BR	Boil up ratio
C_p	Heat capacity (J/kgK)
d	Characteristic length (m)
D_{ij}	Binary diffusion coefficient (m^2/s)
H	Solar irradiance (W/m^2)
H_{sc}	Solar constant (=1367 W/m^2)
H_o	Solar irradiance outside atmosphere (W/m^2)
h_l, h_v	Heat transfer coefficient in liquid and vapor (W/m^2.^{o}C)
HHV	High heating value (MJ/kg)
h'_w	Dimensionless weir height
h_w	Average weir height per liquid pass (m)
I	Investment (M\$)

k_{2t}	Reaction equilibrium constant (m^3/kmol.s)
k^l, k^v	Multicomponent mass transfer coefficient in liquid and vapor (m/s)
L_n	Total molar flow rate of liquid (kmol/s)
MP	Medium pressure steam
M	Molecular weight
$\dot{m}$	Mass flow rate (kg/s)
n	Number of tray
N	Day number (counted from January 1st)
N_A	Component molar flux (mol/s.m^2)
NC	Number of components
P	Pressure (kPa or bar)
PBT	Payback time (year)
Q	Total energy (W)
R	Revenue (M$/year)
R_x	Reaction rate (mol/s.m^3)
Re	Reynolds number
s	Monthly average daily number of hours of bright sunshine (h)
S	Savings (M$/year)
s_0	Day length (h)
Sc	Schmidt number
t	Time (s)
T	Temperature (°C)
$t_{sunrise}$	Sunrise time
t_{sunset}	Sunset time
V	Volume (m^3)
V_n	Total molar flow rate of gas (kmol/s)
V_c	Critical molar volume (cm^3/mol)
x, y	Mole fractions in liquid and vapor phases
λ	Thermal conductivity (W/m. °C)
ρ	Density (kg/m^3)
δ	Solar declination angle
φ	Latitude of the location
ω_{sunset}	Sunset angle
η	Collector efficiency
α	Distribution coefficient

Subscripts

c	Condenser
cold	Cold tank
col	Collector
liq, L	Liquid phase
loss	Lost energy

REFERENCES

1. White, D.C., "Optimize energy use in distillation", ***American Institute of Chemical Engineers,*** Vol. 108, (2012), 37-42.
2. Tora, E.A., El-Halwagi, M.M., "Integration of Solar Energy into Absorption Refrigerators and Industrial Processes", ***Chemical Engineering and Technology***, Vol. 33, No. 9, (2010), 1495-1505.
3. Al-Hasnawi, H., "Solar Heat in Industrial Processes: Integration of Parabolic Trough Solar Collectors in Dairy Plants and Pharmaceutical Plants", Master's thesis, University of UMEA (2015).
4. Pendya, J.D., "Adiabatic gas absorption and stripping with chemical reaction in packed towers", ***Chemical Engineering Communications***, Vol. 19, (1983), 343-361.
5. Pacheco, M.A., Rochelle, G.T., "Rate-based modeling of reactive absorption of CO_2 and H_2S into aqueous methyl-diethanolamine", ***Industrial and Engineering Chemistry Research***, Vol. 37, (1998), 4107-4117.
6. Bolhar, N., Friedl, A., Koss, U., Tork, T., "Modeling selective H_2S absorption and desorption in an aqueous for Australia MDEA-solution using a rate-based non-equilibrium approach", ***Chemical Engineering and Processing: Process Intensification***, Vol. 43, No. 6, (2004), 701-715.
7. Gabrielsen, J., Michelsen, M.L., Stenby, E.H., Kontogeorgis, G.M., "Modeling of CO_2 absorber using an AMP solution", ***A.I.Ch.E. Journal***, Vol. 52, (2006), 3443-3451.
8. Godini, H.R., Mowla, D., "Selective study of H_2S and CO_2 absorption from gaseous mixtures by MEA in packed beds", ***Chemical Engineering Research and Design***, Vol. 86, No. 4, (2008), 401-409.
9. Mostajeran Goortani, B., Gaurav, A., Deshpande, A., Ng, F.T.T., Rempel, G.L., "Production of isooctane from isobutene: energy integration and carbon dioxide abatement via catalytic distillation", ***Industrial and Engineering Chemical Research***, Vol. 54, No. 14, (2015), 3570-3581.
10. Khan, A., Halder, G.N., Saha, A.K., "Comparing CO_2 removal characteristics of aqueous solutions of mono-ethanolamine, 2-amino-2-methyl-1-propanol, methyl-diethanolamine and piperazine through absorption process", ***International Journal of Greenhouse Gas Control***, Vol. 50, (2016), 179-189.
11. Yu, J., Wang, S., Yu, H., "Experimental studies and rate-based simulations of CO_2 absorption with aqueous ammonia and piperazine blended solution", ***International Journal of Greenhouse Gas Control***, Vol. 50, (2016), 135-146.
12. Spek van der, M., Arendsen, R., Ramirez, A., Faaij, A., "Model development and process simulation of post-combustion carbon capture technology with aqueous AMP/PZ solvent", ***International Journal of Greenhouse Gas Control***, Vol. 50, (2016), 176-199.
13. Sherwood, T.K., Holloway, F.A.L., "Performance of packed towers liquid film data for several packings", ***Transactions of the American Institute of Chemical Engineers***, Vol. 36, (1940), 39-70.
14. Onda, K., Takeuchi, H., Okumoto, Y., "Mass transfer coefficients between gas and liquid phases in packed columns", ***Journal of Chemical Engineering of Japan***, Vol. 1, No. 1, (1968), 56-62.
15. Kim, S., Deshusses, M.A., "Determination of mass transfer coefficients for packing materials used in bio-filters and bio-trickling filters for air pollution control", ***Chemical Engineering Science***, Vol. 63, No. 4, (2007), 856-861.
16. Scheffe, R.D., Weiland, R.H., "Mass-transfer characteristics of valve trays", ***Industrial and Engineering Chemical Research***, Vol. 26, No. 2, (1987), 228-236.
17. Goortani, B.M., Heidari, H., "Advanced modeling of CSP plants with sensible heat storage: instantaneous effects of solar irradiance", ***International Journal of Renewable Energy Research***, Vol. 7, No. 3, (2017), 1419-1425.
18. Zhang, J., Zhao, L., Deng S., Xu, W., Zhang, Y., "A critical review of the models used to estimate solar radiation", ***Renewable and Sustainable Energy Reviews***, Vol. 70, (2017), 314-329.
19. Mobtaker, H.G., Ajabshirchi, Y., Ranjbar, S.F., Matloobi M., Taki, M., "Estimation of Monthly Mean Daily Global Solar Radiation in Tabriz Using Empirical Models and Artificial Neural Networks", ***Journal of Renewable Energy and Environment***, Vol. 3, No. 3, (2016), 21-30.
20. Lashkar Ara, A., Hosseini, R., Bagheri Tolabi, H., "Estimation of Global Solar Irradiance Using a Novel Combination of Ant Colony Optimization and Empirical Models", ***Journal of Renewable Energy and Environment***, Vol. 3, No. 3, (2016), 59-66.
21. Yaghoubi, M.A., "Further data on solar radiation in Shiraz, Iran", ***Renewable Energy***, Vol. 7, No. 4, (1996), 393-399.

22. Watanabe, T., Oishi, Y., Nakajima, T.Y., "Characterization of surface solar-irradiance variability using cloud properties based on satellite observations", ***Solar Energy***, Vol. 140, (2016), 83-92.
23. Stefu, N., Paulescu, M., Blaga, R., Calinoiu, D., Pop, N., Boata, R., Paulescu, E., "A theoretical framework for Ångström equation: Its virtues and liabilities in solar energy estimation", ***Energy Conversion and Management***, Vol. 112, (2016), 236-245.
24. Vakili, M., Sabbagh, S.R., Khosrojerdi, S., Kalhor, K., "Evaluating the effect of particulate matter pollution on estimation of daily global solar radiation using artificial neural network modeling based on meteorological data", ***Journal of Cleaner Production***, Vol. 141, (2017), 1275-1285.
25. Peng, D.Y., Robinson, D.B., "A New Two-Constant Equation of State", ***Industrial and Engineering Chemistry: Fundamentals***, Vol. 15, (1976), 59-64.
26. Wilke, C.R., Chang, P., "Correlation of diffusion coefficients in dilute solutions", ***A.I.C.H.E. Journal***, (1955), 264-270.
27. Harmens, A., Knapp, H., "Three parameter cubic equation of state for normal substances", ***Industrial and Engineering Chemistry Fundamentals***, Vol. 19, (1980), 291-294.
28. Barbero, R., Rovira, A., Montes, M.J., Martínez Val, J.M., "A new approach for the prediction of thermal efficiency in solar receivers", ***Energy Conversion and Management***, Vol. 123, (2016), 498-511.
29. Cocco, D., Serra, F., "Performance comparison of two tanks direct and thermocline thermal energy storage system for 1MWe class concentrating solar power plants", ***Energy***, Vol. 81, (2015), 526-536.
30. Bird, R.B., Stewart, W.E., Lightfoot, E.N., "Transport Phenomena", (1960).